Bioelectrochemistry 128 (2019) 263–273

Contents lists available at ScienceDirect

Bioelectrochemistry

journal homepage: www.elsevier.com/locate/bioelechem

A bombykol electrochemical receptor sensor and its kinetics

Dingqiang Lu [a,b,1], Qiuda Xu [a,b,1], Guangchang Pang [a,*]

[a] College of Biotechnology & Food Science, Tianjin University of Commerce, Tianjin 300134, China
[b] Tianjin Key Laboratory of Food Biotechnology, Tianjin 300134, China

ARTICLE INFO

Article history:
Received 1 December 2018
Received in revised form 9 April 2019
Accepted 9 April 2019
Available online 23 April 2019

Keywords:
Bombykol
Electrochemical receptor biosensor
Electrochemical signal amplification system
GPCRs
Ligand interaction kinetics

ABSTRACT

This study aimed to explore the interaction between bombykol and BmOR1 and also provide a paradigm for agroforestry pest control. The electrochemical biosensor signal amplification system was used: nanogold with horseradish peroxidase. An electrochemical bilayer nanogold membrane receptor sensor was developed using the following schemes and processes: twice self-assembly of nanogold and succeeding absorption of *Bombyx mori* olfactory receptor 1 (BmOR1); sex pheromone–binding protein; spectral scanning and transmission electron microscope to characterize nanogold sol; and atomic force microscope, cyclic voltammetry, and AC impedance methods to characterize individual processes of sensor assembly. The amperometric *I–T* curve was adopted to measure the response current upon interaction with different concentrations of bombykol (diluted in phosphate-buffered saline) and BmOR1. The results demonstrated the receptor–ligand interaction pattern, which was similar to enzymatic reaction kinetics, with the activation constant *Ka* of up to 8.57×10^{-20} mol/L and signal magnification of about 10,000-fold. In this study, the simulation of intracellular receptor signaling cascade by an electrochemical signal amplification system helped in directly measuring BmOR1–bombykol ligand interaction and exploring the kinetics after the self-assembly of BmOR1 on the biosensor. It provided a novel platform for future studies on receptor–ligand interaction.

1. Introduction

Bombykol, an insect sex pheromone, is secreted mainly by female silkworm moths [1,2]. It is a natural ligand of *Bombyx mori* pheromone–binding protein(PBP) [3]. Bombykol is transported to the membrane surface of dendrites upon binding with PBP and interacts with the membrane receptor protein. G protein–coupled receptor (GPCR), the membrane receptor for bombykol, resides on the membrane of sensory neuron axons [4,5]. Upon binding of the extracellular domain with bombykol, the receptor couples to intracellular G protein via complicated conformational changes in seven transmembrane domains and cascade effects [6], selectively activating multiple downstream signaling cascades and generating nerve impulses and receptor potentials by depolarization [7–9].

GPCRs, a receptor superfamily constituted by thousands of members, have a critical role via complex intracellular signaling pathways in systemic/cellular substance metabolism, energy metabolism, and signaling communication [10]. At present, studies related to ligand–receptor interaction focus mainly on the extracellular domain of receptor and binding domain of ligand and on the application in drug screening. For GPCR-based drug screening, the live cell assay platform [11] comprising high-throughput screening assays, cell microarrays, and cell microfluidics is mostly used. It shows a high degree of miniaturization and multifunctionality under low-cost conditions [12,13]. Also, cells expressing exogenous GPCR target proteins are easy to manipulate. However, they may not represent the true situation of the target cells in the natural environment [14]. Moreover, new detection methods are based on label-free systems, such as surface plasmon resonance, resonance waveguide grating, impedance [15–17], or surface acoustic wave sensors [18].

These methods directly measure GPCR–ligand interactions, independent of the binding site, probe, and signaling pathway. They are useful for primary and orthogonal screening and overcome the limitations of indirect and displacement assay methods [19]. Overall, these methods are based on the receptor–ligand interaction. They are obviously useful, hypersensitive, and label-free techniques for the antigen–antibody interaction, DNA–RNA molecular probe hybridization, and affinity analysis of aptamers. However, they are inappropriate for the analysis of catalytic activity of enzymes, signal recognition by the extracellular domain of receptors, and intracellular signal transduction and amplification, even generating the opposite results. According to the previous studies on signal transduction of ligand recognition and intracellular amplification via receptors, which was detected with live cell assay platform [20], the process of signal recognition and amplification was similar to the enzyme–substrate catalysis. The *Km* value of enzymes is known to negatively correlate with their catalytic efficiency,

* Corresponding author.
E-mail address: pgc@tjcu.edu.cn (G. Pang).
[1] Co-first author.

https://doi.org/10.1016/j.bioelechem.2019.04.009
1567-5394/

indicating that the smaller the *Km* value (the greater affinity of the enzyme with the substrate), the smaller the concentration of substrate (ligand) upon reaching the 1/2 maximum catalytic reaction rate, and the more the effectiveness.

Silkworms can sense bombykol secreted from female silkworm moths from miles away. This indicates that the natural olfactory signal amplification system of the silkworms is quite efficient and sensitive [21]. The interaction of olfactory receptors with odor molecules/sex pheromones is a good study subject for receptor–ligand interactions. Therefore, an electrochemical signal amplification system based on nanogold and horseradish peroxidase (HRP) was designed, aiming to simulate the intracellular signal amplification system, thereby further probing the receptor–ligand interaction pattern (Scheme 1). The heterotrimeric G proteins function as transducers to activate many signaling pathways. When the guanosine diphosphate (GDP) on the Gα subunit was replaced with guanosine triphosphate (GTP), the complex dissociated into Gα/GTP and Gβγ subunits, which were then capable of activating or inhibiting a wide range of signaling systems. This study designed an electrochemical signal amplification system based on gold nanoparticles (AuNPs) and HRP to simulate the intracellular signal amplification system for the study of the receptor–ligand interaction.

The proposed *B. mori* olfactory receptor 1 (BmOR1) biosensor was schemed using the following strategy. Bombykol binds to the BmOR1 sensor, on which multiple thiol groups of the intracellular domain bind to AuNPs. Also, the electrochemical signal changes, generated by the interaction of the extracellular domain of receptor with the ligand, are further amplified through HRP. The results demonstrated that the biosensor could not only supersensitively detect bombykol but also simulate intracellular signal cascade amplification of receptors, benefiting studies on the kinetics pattern of receptor–ligand interaction.

2. Experimental

2.1. Reagents and solutions

B. mori was procured from Jilin Provincial Sericultural Sericulture Academy of Science (China). Bombykol was obtained from Hangzhou FandaChem (China); Chitosan (chitosan, Chit, deacetylation degree ≥90%) from Jinan Haidebei Marine Biological Engineering Co., Ltd. (China); sodium citrate from Tianjin Winda Rare Chemical Reagent Factory (China); chloroauric acid from Shenyang Jinke Reagent Factory (China); bovine serum albumin (BSA) and Tween-20 from Sigma (USA); thionin acetate (Thi) from Sigma–Aldrich (USA); and HRP (1000 units/mg) from Solarbio (Beijing, China). A total of 0.1 g/100 mL Chit solution was used: 0.1 g Chit dissolved in 100 mL of 1% acetic acid solution. The reagents used were of analytical grade, and the water used in the experiments was ultrapure water (18.2 MΩ/cm).

2.2. Apparatus

The CHI 660E electrochemical workstation and the three-electrode system were purchased from Shanghai Chenhua Instrument Co., Ltd. (China). Among them, Ag/AgCl was used as the reference electrode, platinum wire electrode (Pt) as the counter electrode, and glassy carbon electrode (GCE, $\varphi = 3$ mm) as the working electrode. A KQ 3200B ultrasonic cleaner was procured from Kunshan Ultrasonic Instrument Co., Ltd. (China) and used for GCE pretreatment. A microwave oven was purchased from the LG Company (Korea). A UV-2501 ultraviolet-visible (UV–Vis) spectrophotometer was obtained from Shimadzu Instrument Co., Ltd. (Japan). A DHG-907385-III CIMO electric heating constant-temperature air-drying oven was purchased from Haixin Miao Medical Device Manufacturing Co., Ltd. (China) An atomic force microscope (AFM) Dimension 3100 was procured from Veeco (USA). The tapping mode was used to characterize the different modification stages of the electrodes. A transmission electron microscope (TEM; Philips Tecnai G2F20, Netherlands) with an acceleration voltage of 200 kV was used to characterize AuNPs.

2.3. Preparation of Thi/Chit copolymer, AuNPs, and AuNPs/HRP

The thiopurine/Chit copolymers were prepared using the reference method [23] with improvement. Then, 2.5 mL of 2% (*w*/*v*) Chit solution (2 g of Chit in 100 mL of 2% *v*/v acetic acid solution mixed for 3 h) was added to 320 μL of 10% glutaraldehyde (*v*/v) solution. After mixing, 200 μL of 0.01 mol/L thionine (Thi) solution was added to the aforementioned solution, and finally, 2% (*v*/v) acetic acid solution was added to a

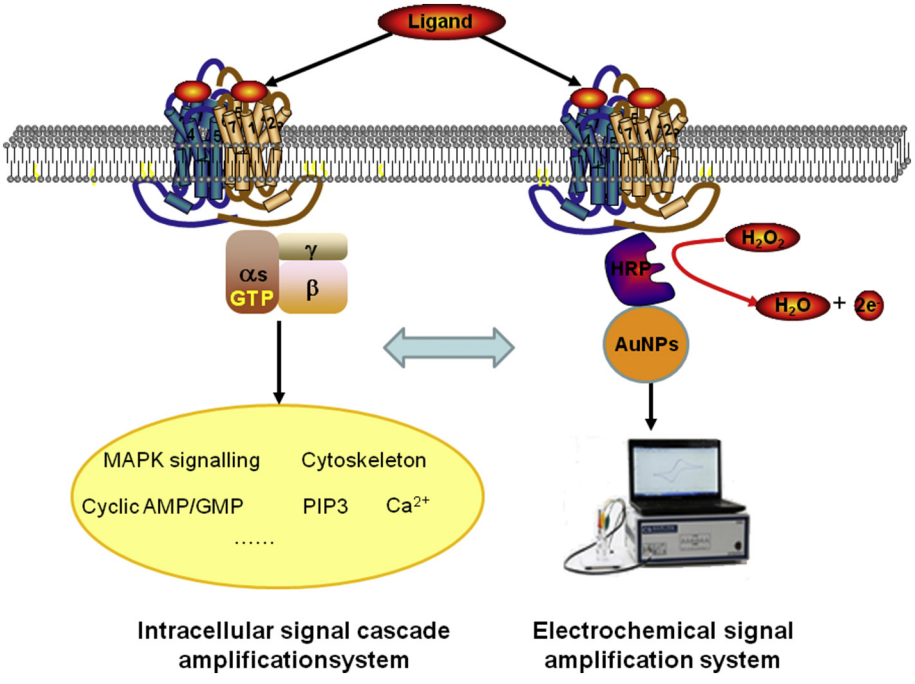

Scheme 1. Electrochemical signal amplification system simulating the intracellular signal amplification system.

total volume of 6 mL. After mixing, the solution was used for dispensing electrodes.

In this study, trisodium citrate was used to reduce chloroauric acid for preparing AuNPs, following the Frens method [24]. Subsequently, 4 mL of 1 g/100 mL of trisodium citrate was added to a neutral 100 mL of 0.01 g/100 mL chloroauric acid solution. The solution was placed in a microwave oven and heated until it became bright red wine in color (about 10–20 min). After cooling, ultrapure water was added to the original volume, and the solution was stored at 4 °C for further use. The AuNP sols were characterized using UV–Vis spectrophotometry and transmission electron microscopy.

According to the previous methods [25], 0.1 mol/L K_2CO_3 was used to adjust the pH of the prepared AuNPs sol to 7.0. Then, 1 mL of AuNP sol was mixed with 1 mL of 2.0 g/L HRP solution [0.01 mol/L, pH 7.4, phosphate-buffered saline (PBS) solution], stirred for 2 h, and stored at 4 °C overnight for further use.

2.4. Extraction of BmOR1

BmOR1 protein was extracted according to the manual of the protein extraction kit (KeyGen Biotech), with minor modifications. Specifically, 25 pairs of antennas were collected from male silkworm moths (virgin) after eclosion. The antennas were ground in a beaker using a pestle with the slow addition of 1 mL of lysis buffer (containing 5 μL of a phosphatase inhibitor, 1 μL of a protease inhibitor, and 10 μL of phenylmethylsulfonyl fluoride) using a pipette. The ground tissue was homogenized 30–50 times using a glass homogenizer (on ice for the entire process to prevent heat denaturation of proteins), prior to placing on ice for about 5 min. Then, the homogenate was transferred to a prechilled centrifuge tube to spin at 4 °C for 5 min at 13,000 rpm, and the supernatant was transferred to a new centrifuge tube as the protein extract.

2.5. Fabrication of the bombykol electrochemical olfactory receptor biosensor and detection principle

GCE was pretreated using conventional methods. It was sequentially polished on the suede with an α-Al_2O_3 paste of 1.0, 0.3, and 0.05 μm particle size and then washed in an ultrasonic water bath for 30 s after each polishing. This process was repeated thrice. Finally, the samples were washed with a 1:1 ratio of HNO_3, absolute ethanol, and ultrapure water. A cyclic voltammetry–activated electrode with a scan range of 1.0–1.0 V and a sweep rate of 100 mV/s in 1 mol/L H_2SO_4 solution was used to repeatedly scan until a stable cyclic voltammetry curve appeared. The recorded cyclic voltammetry curves in 1 mmol/L $K_3Fe(CN)_6$ solution (containing 0.20 mol/L KNO_3) were used to characterize the pretreatment effect of GCE with a scan range of 0.6–0.1 V and a scan speed of 50 mV/s. The electrode was used unless the peak potential difference of the cyclic voltammetry curve of the pretreated electrode under laboratory conditions was <80 mV, approximately 64 mV, and finally the electrode was placed in a nitrogen atmosphere for drying.

An electrochemical biosensor with a signal amplification system was developed using a previously reported method [26,27] (Scheme 2). After the pretreatment of GCE, 5 μL of 0.5% Chit solution (0.5 g of Chit dissolved in 100 mL of 1% acetic acid solution) was dropped on the surface of the electrode, dried in an oven at 45 °C for 3 h, and cooled to room temperature. Then, it was immersed in 1 mol/L NaOH solution for 5 min, subsequently washed with ultrapure water, and immersed in ultrapure water for 30 min (step 1). It was then taken out, naturally dried, and placed in AuNPs sol for 24 h (step 2). Subsequently, the electrode was placed in 1 mg/mL BmOR1 extraction solution at 4 °C for self-assembly for 24 h to obtain a single-layer AuNP-modified sensor (step 3). Further, 5 μL of the prepared Thi/Chit copolymer solution was added dropwise to the center of the electrode surface. After drying naturally, the polymer film was repeatedly washed with ultrapure water until the water had no absorbance at 600 nm, following which the electrode was placed in the AuNPs/HRP solution at 4 °C for self-assembly for 24 h (step 4). After washing with ultrapure water, the electrode was placed in 1 mg/mL BmOR1 extraction solution at 4 °C for self-assembly for 24 h (step 5). Finally, the modified electrode was placed in the BSA solution (1 g/100 mL) for 1 h at 37 °C to block nonspecific sites, and unbound BSA was washed with PBS and Tween 20 solution containing 0.05% (*v*/v) Tween-20 (step 6). The film was naturally dried to obtain an electrochemical nanobiosensor, and then the electrode was placed in the PBS buffer at 4 °C for further use.

A three-electrode system on the receptor sensor was used to determine the silkworm moth alcohol. The current–time scanning was performed at an optimized potential to vary the steady current values (I_1 and I_2) before and after the reaction for a quantitative determination of silkworm moth alcohol. The reaction principle was based on the combination of HRP and Thi on GCE to produce a series of redox reactions with H_2O_2.

$$\mathrm{HRP} + \mathrm{H_2O_2} \rightarrow \mathrm{Compound\ I} + \mathrm{H_2O}. \quad (1)$$

$$\mathrm{Compound\ I} + \mathrm{Thi\ (red)} \rightarrow \mathrm{Compound\ II} + \mathrm{Thi\ (ox)}^{*}. \quad (2)$$

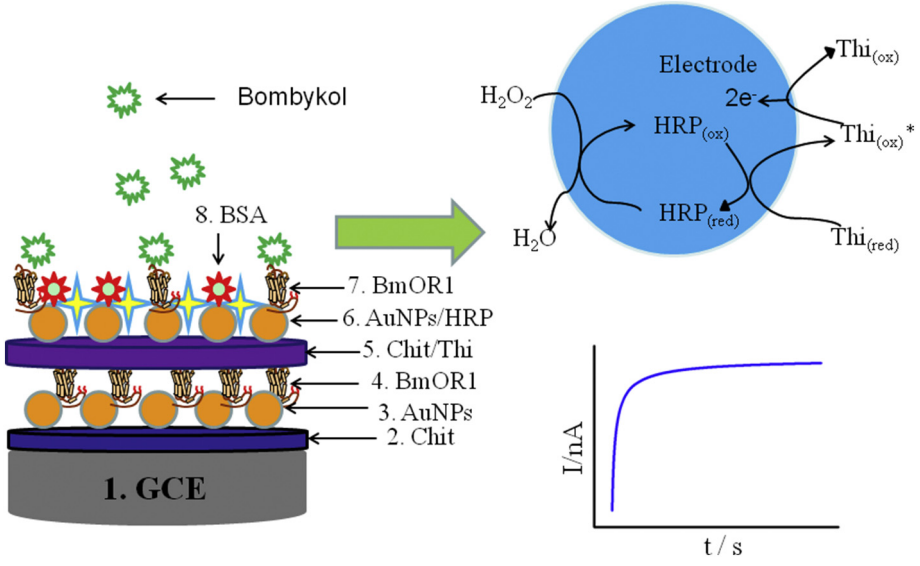

Scheme 2. Schematic illustration of the fabrication of BmOR1 biosensors.

$$\text{Compound II} + \text{Thi (ox)}^{*} + 2H^{+} \rightarrow \text{HRP} + \text{Thi (ox)} + H_2O. \quad (3)$$

$$\text{Thi (ox)} + 2e^{-} + 2H^{+} \rightarrow \text{Thi (red)}. \quad (4)$$

The ligand complex on the electrode surface blocked electron transfer due to steric hindrance, and the change in the steric effect could be measured by the change in the current. The concentration of the ligand could be detected by detecting the change in the current before and after binding of the ligand.

2.6. Use of BmOR1 biosensors

A three-electrode working system was adopted: assembled BmOR1 biosensors as the working electrode; Ag/AgCl electrode as the reference electrode; and Pt as the counter electrode. Taking ultrapure water (18.2 MΩ/cm) as the blank control, the amperometric *I–T* curve was adopted at a certain voltage to measure the response current upon its interaction with different concentrations of bombykol and BmOR1, and the change rate of response currents was taken as the measurement variable (H_2O_2 pre-added to reach the final concentration of 8 mmol/L). Given that bombykol is soluble in organic solvents, it was dissolved in 75% ethanol to prepare the mother liquor at a concentration of 1 mol/L and preserved at 4 °C. The working concentration was prepared by dilution in ultrapure water right before use.

The change rate in response current was calculated using the following equation:

$$\Delta I/\% = \frac{I1 - I2}{I1} \times 100 \quad (5)$$

Note: I_1 and I_2, respectively, represent the values of steady-state current at the same time points as bombykol response current (pre- and post-measurements).

3. Results and discussion

3.1. Characterization of AuNPs

The synthesized AuNPs in this study were bright red wine in color. The scanning spectra in the wavelength range of 400–700 nm are shown in Fig. 1. The result showed a strong absorption peak at 521 nm, roughly indicating that the average particle size of AuNPs was 15–20 nm. The TEM results of AuNPs are shown in Fig. 1B and C. The figure shows that the synthesized AuNPs in this study had a regular shape, uniform particle size, and average particle size of about 15 nm with no aggregation. The characterization of AuNPs using UV–Vis spectra was the same as that using TEM scanning, suggesting that the particle size of AuNPs was 15–20 nm, which could be used for subsequent experiments.

3.2. Pretreatment characterization of the electrode

Fig. 2A shows the cyclic voltammograms of GCE before and after the pretreatment. After preprocessing, its redox peak current increased significantly. The peak potential difference was <80 mV and the peak current ratio close to 1 (the electrode after H_2SO_4 activation produced negatively charged oxygen-containing groups on the surface, such as hydroxyl and carboxyl [28], and also formed a porous structure, increasing the effective surface area [29]), suggesting that the electrode met the requirements. Fig. 2B shows the cyclic voltammogram of the electrode at different scanning rates (1 → 8 successively: 25, 50, 75, 100, 125, 150, 200, and 250 mV/s) (scanning range: 0.6–0.1 V). The embedded Fig. 2C in 2B shows that the redox peak current exhibited a good linear relationship with the square root of sweep speed, indicating that the redox peak current of the electrode was controlled only by diffusion.

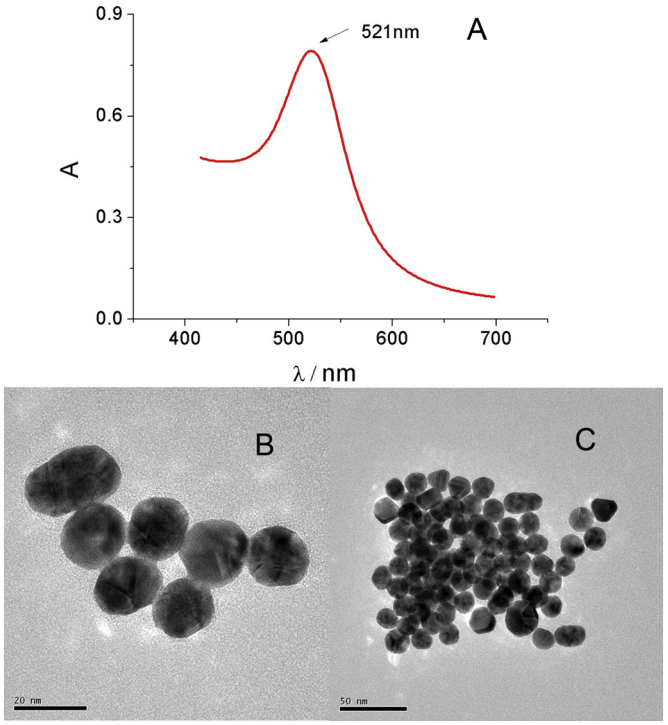

Fig. 1. (A) Spectral absorption curve of GNPs. The TEM image of GNPs at (B) 1 × 145,000 and (C) 1 × 71,000.

GCE in this study received a good pretreatment effect, and the performance of the electrode was improved by H_2SO_4 activation, which could be used in subsequent studies.

(a–h) GCE, Chit-GCE, GNPs-Chit-GCE, BmOR1-GNPs-Chit-GCE, Thi/Chit-BmOR1-GNPs-Chit-GCE, HRP/GNPs-Thi/Chit-BmOR1-GNPs-Chit-GCE, BmOR1-HRP/GNPs-Thi/Chit-BmOR1-GNPs-Chit-GCE, and BSA-BmOR1-HRP/GNPs-Thi/Chit-BmOR1-GNPs-Chit-GCE.

Abbreviations: BSA, bovine serum albumin; BmOR1, bombykol receptor protein; chit, chitosan; GCE, glassy carbon electrode; GNPs, gold nanoparticles; HRP, horseradish peroxidase; Thi, thionine

3.3. Electrode assembly and characterization

Fig. 2D and E shows the cyclic voltammetry characterizations of the bombykol electrochemical olfactory receptor biosensors at different assembly stages in 1×10^{-3} mol/L $K_3Fe(CN)_6$ (containing 0.20 mol/L KNO_3) solution, with a scanning range of 0.6–0.1 V and a scanning speed of 50 mV/s.

In Fig. 2, the curves a, b, c, d, e, f, g, and h represent eight different modification stages of bare GCE, Chit-GCE, GNPs-Chit-GCE, BmOR1-GNPs-Chit-GCE, Thi/Chit-BmOR1-GNPs-Chit-GCE, HRP/GNPs-Thi/Chit-BmOR1-GNPs-Chit-GCE, BmOR1-HRP/GNPs-Thi/Chit-BmOR1-GNPs-Chit-GCE, and BSA-BmOR1-HRP/GNPs-Thi/Chit-BmOR1-GNPs-Chit-GCE, respectively.

Comparison between curves a and b shows that the peak current of the cyclic voltammogram decreased and the impedance increased significantly after the Chit film assembled on the bare GCE electrode because the Chit film hindered the electron transfer, confirming that it was successfully assembled. The curve c shows that the redox peak current of assembled GNPs increased sharply and the impedance decreased sharply because the tunneling effect of GNPs and the excellent electron transport ability accelerated electron transfer. The redox peak current shown in curve d was significantly smaller than that shown in curve c, while the impedance significantly increased because the lower conductivity of BmOR1 protein molecule and the steric hindrance effect on the electrode hindered the transfer of electrons, indicating that the BmOR1

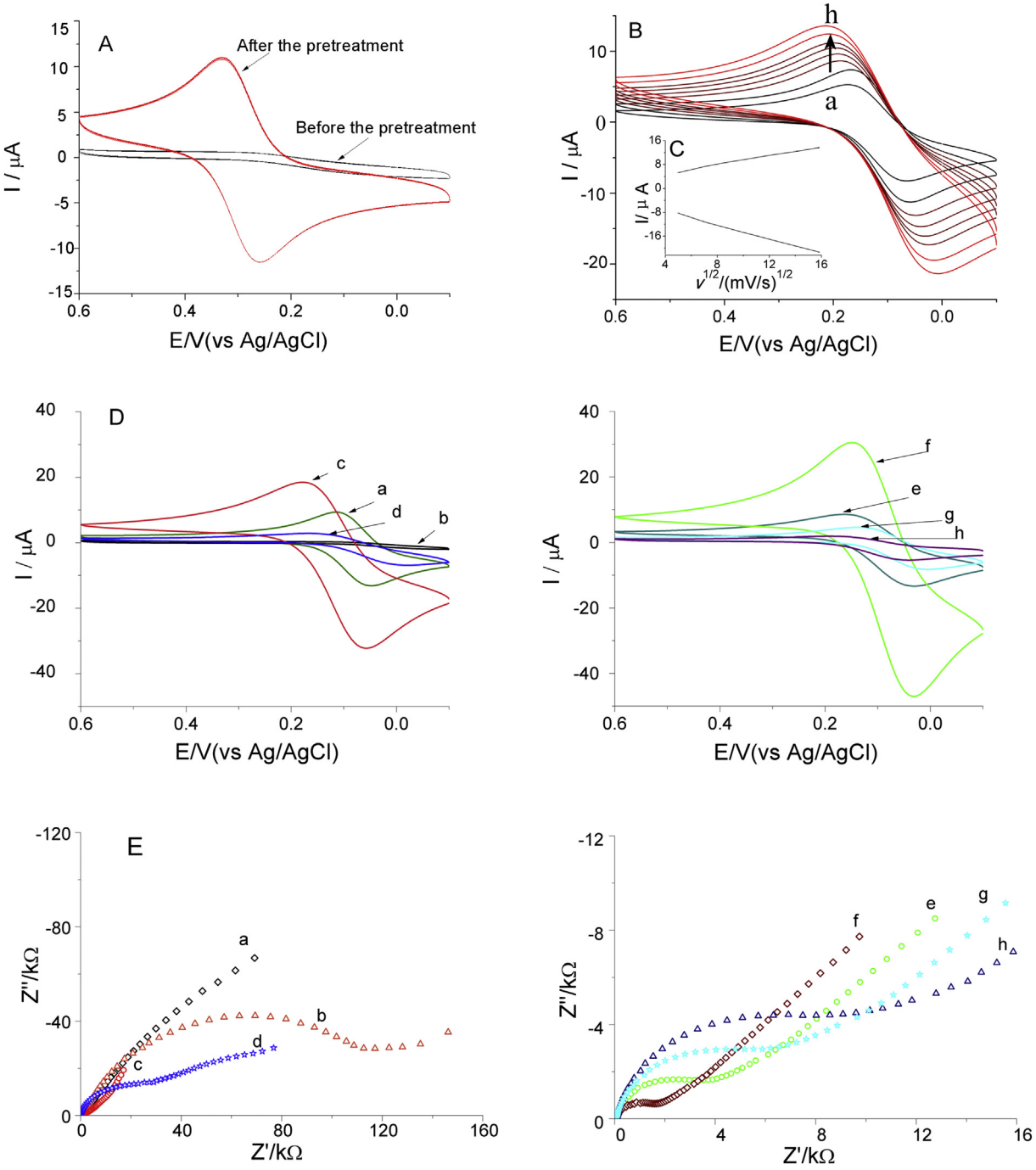

Fig. 2. Characterization of the effect of the GCE pretreatment: (A) cyclic voltammetry; (B) cyclic voltammograms of bare GCE at scan rates of 0.025, 0.050, 0.075, 0.100, 0.125, 0.150, 0.200, and 0.250 V/s (a → h); (C) the inset shows the dependence of the redox peak currents on the square root of scan rates (Correlation coefficients $R^2 = 0.9873$, $R^2 = 0.9894$); and (D and E) characterized electrode in the modifying process by cyclic voltammetry and AC impedance; both CV and AC impedance performed in 1 mmol/L $K_3Fe(CN)_6$ solution containing 0.20 mol/L KNO_3.

was successfully assembled. Curve e shows that the redox peak current of assembled Thi/Chit polymer slightly increased and the impedance slightly reduced compared with those in curve d, which might be because the contribution of Thi to promote electron transfer was greater than the effect of Chit on electron transfer inhibition. Curve f shows the electrochemical characterization of the second layer of gold (adsorbed with HRP). The redox peak current increased, and the impedance decreased significantly. This might be due to the greater contribution of GNPs to electron transfer. The redox peak current in curve g significantly reduced and the impedance increased compared with that in curve f, indicating that the second layer of BmOR1 assembled on the electrode. The redox peak current shown by curve h further decreased and the impedance increased, indicating that the BSA blocked the electrode surface nonspecific sites.

Moreover, the characterization with AFM, via the roughness (Ra) of membrane surfaces before and after assembly, directly displayed the scenarios of biosensor assembly and then biosensor binding to bombykol after successful assembly (shown in Fig. 3).

Table 1 lists the parameters of electrode surface morphology. Nanoscope 6.11r1 was used to analyze the data. Compared with the bare electrode (Fig. 3A), the Ra reduced from 3.18 to 0.52 nm after Chit drying and membrane formation (Fig. 3B), because the Chit

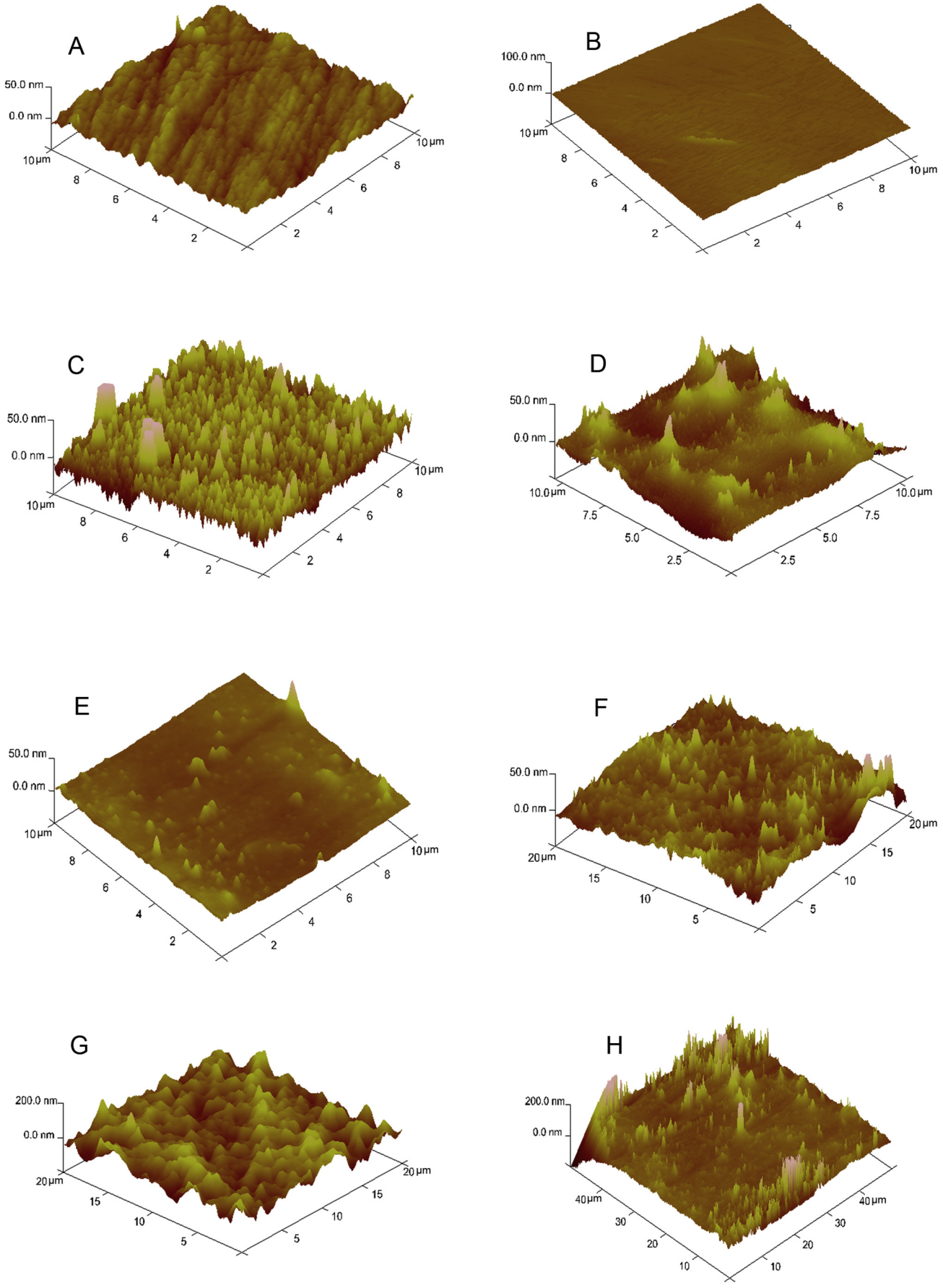

Fig. 3. AFM characterization of the electrode assembly by the tapping mode. (A–H) GCE, Chit-GCE, GNPs-Chit-GCE, BmOR1-GNPs-Chit-GCE, Thi/Chit-BmOR1-GNPs-Chit-GCE, HRP/GNPs-Thi/Chit-BmOR1-GNPs-Chit-GCE, BmOR1-HRP/GNPs-Thi/Chit-BmOR1-GNPs-Chit-GCE, and BSA-BmOR1-HRP/GNPs-Thi/Chit-BmOR1-GNPs-Chit-GCE.

membrane covered the scratch of the bare electrode, and the peak depth reduced from 90.5 to 3.18 nm. After AuNPs adsorption (Fig. 3C), Ra increased from 0.52 to 8.11 nm because Au nanoparticles showed spherical shape, uniformly covering the surface of smooth membrane and increasing Ra. Moreover, the peak depth also increased from 3.18 to 100.22 nm. After BmOR1 self-assembly (Fig. 3D), Ra continuously increased because Au adsorbed many BmOR1 proteins by Au—S. The peak depth also increased. After mixing Thi–Chit with sol and forming a membrane (Fig. 3E), Ra decreased from 15.3 to 3.01 nm due to the same reason, and the peak depth decreased to half of the membrane potential after BmOR1 self-assembly. Afterward, the electrode was placed in an AuNPs–HRP mixing solution and immersed overnight for self-adsorption (Fig. 3F). The existence of Au particles and HRP increased Ra slightly (3.01–4.44 nm). After the second adsorption of a large amount of BmOR1 protein (Fig. 3G), Ra increased by about six times, and the peak depth increased two times (Ra increased from 4.44 to 25.6 nm; peak depth increased from 70.6 to 143.3 nm). Finally, BSA was used to block the Au nanoparticles that did not bind with BmOR1 molecules (Fig. 3H). Ra reduced, and the peak depth slightly decreased (Ra decreased from 25.6 to 15.2 nm; peak depth decreased from 143.3 to 128.3 nm). The assembly of sensor was finished, and it was stored at 4 °C in 0.01 M PBS (pH 7.4) for further detection.

3.4. Optimization of detection conditions for BmOR1 biosensors

3.4.1. Optimization of detection potential

The amperometric *I–T* curve was adopted to measure the response current upon its interaction with bombykol at different potentials. Taking ultrapure water as the blank control, 10^{-15} mol/L bombykol was added to the test group, and the change rate of steady-state currents was measured to evaluate the effect of different potentials on the response effectiveness of this electrochemical biosensor. The results demonstrated that the current change rate reached a maximum at a potential of −0.4 V (Fig. 4A). Therefore, a constant potential at −0.4 V was chosen for the study of biosensor response characteristics to bombykol.

3.4.2. Optimal test time

Fig. 4B displays the response currents generated by the binding of BmOR1 biosensors to 10^{-15} mol/L bombykol ligand at different time. The chosen time scheme was as follows: the time of binding response was 3–21 s, and the interval was 3 s. The comparisons indicated that the change rate of electrode signal currents was basically stable in 9 s. Therefore, the optimal test time for receptor–ligand binding was determined to be 10 s, following which the current values were stable.

3.4.3. H_2O_2 concentration

Fig. 4C reveals that the addition of different concentrations of H_2O_2 influenced the change rate of response currents in BmOR1 biosensors. When the H_2O_2 final concentration was <8 mmol, the current change rates gradually rose with an increase in additional volumes, whereas they were stable after the H_2O_2 final concentration reached 8 mmol, indicating that 8 mmol could be taken as the optimal supplement dose.

3.4.4. Response current–time

Fig. 4D displays response currents upon addition of different concentrations of bombykol (10^{-19}–10^{-14} mol/L) at different times. The response current was stable at 30 s. Hence, the current at 30 s was taken as the steady-state current.

3.5. Kinetic curve of bombykol–BmOR1 interaction

The amperometric *I–T* curve was adopted to test assembled electrodes. The logarithm of concentration (lg*C*) was taken as the horizontal ordinate, while the change rate of response currents was taken as the vertical ordinate to plot the curve due to the wide spectrum of bombykol concentration, which made plotting difficult. As shown in Fig. 5A, the change rate of response currents showed an optimal linear correlation with increasing bombykol concentrations within the concentration range of 10^{-19}–10^{-14} mol/L.

Table 1
Surface roughness, peak height, and peak spacing during electrode assembly.

Assembly step	Ra value (nm)	Peak depth (nm)	Peak to peak distance (nm)
A	3.18	90.5	1.32
B	0.52	3.18	1.14
C	8.11	100.22	0.81
D	15.3	126.7	1.34
E	3.01	51.7	1.21
F	4.44	70.6	1.68
G	25.6	143.3	2.61
H	15.2	128.3	2.13

Ra, Roughness.

A concentration range of 10^{-19}–10^{-16} mol/L of bombykol was chosen based on the linear range, as shown in Fig. 5A. The test concentrations were further subdivided for plotting (Fig. 5B), using concentrations of test substance (bombykol) as the horizontal ordinate and the change rate of currents as the vertical ordinate.

Based on the receptor–ligand binding kinetic equation:

$$[R] + [L] \underset{k_1}{\overset{k_2}{\rightleftarrows}} [RL] \tag{6}$$

When the receptor was saturated:

$$Kd = \frac{k1}{k2} = \frac{[R][L]}{[RL]} \tag{7}$$

If [*RT*] was designated as the initial concentration of the receptor, then [*R*] = [*RT*] – [*RL*]; if [*LT*] was the total ligand concentration, then [*L*] = [*LT*] – [*RL*]; after substitution of [*L*] = [*LT*] – [*RL*]/[*R*] = [*RT*] – [*RL*] into Eq. (7), the new equation was as follows:

$$[RL]^2 - [RL]\{[RT] + [LT] + Kd\} + [RT][LT] = 0 \tag{8}$$

The aforementioned equation is a hyperbolic quadratic equation with one unknown, [*RL*] being the variate. When [*RT*]/*Kd* was fixed, [*RL*] varied with changes in [*LT*], rapidly rising at the beginning, and then gradually reaching the horizontal level, which was the saturation curve of receptor–ligand interaction. The equation indicates that the receptor–ligand binding had a ligand saturation effect, similar to the enzyme–substrate interaction. The substrate saturation effect was the signature of enzyme catalysis.

Software Origin 8.0 was applied to make a hyperbolic fitting for curves in Fig. 5B, and the acquired new curve is shown in Fig. 5C, with the following fitting equation:

$$\Delta I = 4.2046 \times 10^{-20} C / \left(1.0299 + C \times 10^{-19}\right) \ (R2 = 0.9526) \tag{9}$$

Fig. 5C and the aforementioned fitting equation show that the curve of test substance–receptor interaction conformed to the hyperbola, with the substrate saturation effect similar to enzyme–substrate interaction kinetics.

Fig. 5B shows that the current change rates increased with increases in test substance (bombykol) concentrations, indicating that BmOR1 receptor had not reached saturation yet. However, after reaching a certain concentration, the test substance (bombykol) concentration kept rising, while the current change rates hardly or slightly changed. This indicated that the BmOR1 receptor had already reached saturation. The aforementioned process and hyperbolic fitting results/equation indicated that the biosensor not only reflected the binding of BmOR1 receptor with the

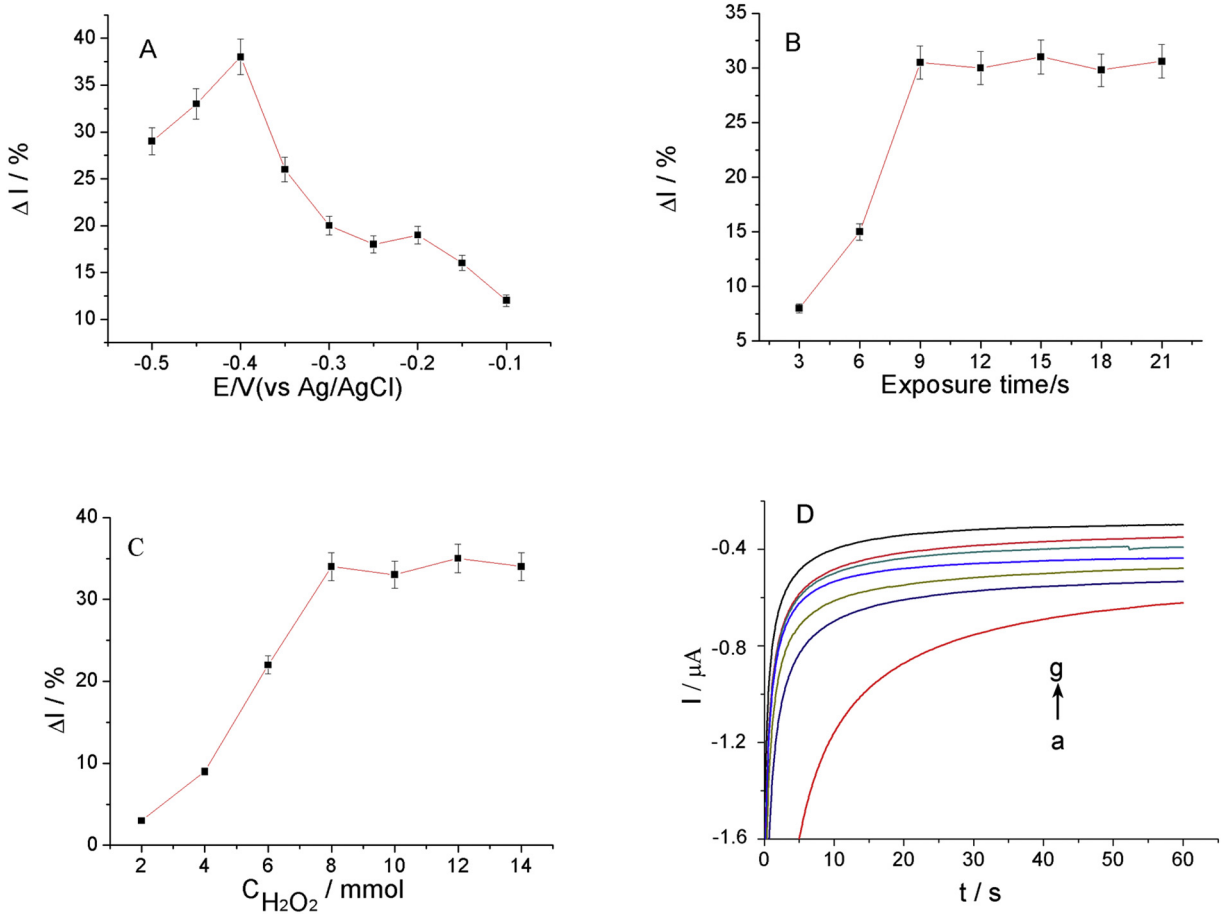

Fig. 4. (A) Current rate change of the biosensor at different voltages in ultrapure water containing 10^{-15} mol/L bombykol. (B) Current rate change of the biosensor for different time in ultrapure water containing 10^{-15} mol/L bombykol. (C) Current rate change of the biosensor at different doses of H_2O_2. (D) Response current of the biosensor at different times (concentrations of bombykol: 10^{-19}–10^{-14} mol/L).

ligand but simulated in vivo signal transduction following the receptor–ligand binding.

When $[R] = [RT] - [RL]$ was substituted in Eq. (7), the resulting equation was as follows:

$$Kd = \frac{\{[RT] - [RL]\}[L]}{[RL]} \tag{10}$$

$$Kd[RL] = [RT][L] - [RL][L] \tag{11}$$

Eq. (11) was transformed as follows:

$$\frac{1}{[RL]} = \frac{1}{[RT]} + \frac{Kd}{[RT]}\frac{1}{[L]} \tag{12}$$

The aforementioned equation is the Lineweaver–Burk equation (also named as double reciprocal equation). A straight-line diagram was plotted, with $1/[RL]$ as the vertical axis and $1/[L]$ as the horizontal axis, $Kd/[RT]$ as the slope of the straight line, $-1/Kd$ as the horizontal axis intercept, and $1/[RT]$ as the vertical axis intercept. According to the aforementioned deduction, a diagram was plotted (double reciprocal plot), with the reciprocal of bombykol concentration being the horizontal axis and the current change rate being the vertical axis (Fig. 5C). The linear regression equation of fitting was as follows:

$$\frac{1}{\Delta I} = 2.01 \times 10^{-19}\frac{1}{C} + 2.3445 \left(R^2 = 0.9768\right) \tag{13}$$

$$Kd = \frac{2.01 \times 10^{-19}}{2.3445} = 8.57 \times 10^{-20}\ mol/L \tag{14}$$

Bombykol signal amplification constant *Ka* (*Kd* in the aforementioned equation) was 8.57×10^{-20} mol/L. The activation constant *Ka* was similar to the enzyme catalysis parameter *Km*. It was defined as the ligand concentration when the 1/2 maximum biological effect of receptor saturation was achieved. The smaller the *Ka* value, the greater the biological efficiency generated by the receptor–ligand interaction. Misawaf and coworkers [30] combined the use of *Xenopus laevis* oocytes and fluidic devices to develop a highly sensitive and selective odorant sensor using oocytes capable of expressing insect olfactory receptors. The system can be applied to detect odorants and pheromones. These receptors are known to be involved in the regulation of ion flow through plasma membranes by selective recognition of the corresponding pheromones or odorants, bombykol, bombykal, Z11–16:Ald, and 2-heptanone. The advantages of this assay were easy processing, hypersensitivity, and high specificity; the disadvantage was a typical short lifespan associated with cell-based biosensors. Mitsuno and coworkers reported the development of a novel cell-based odorant sensor element that sensitively and selectively detected odorants and displayed increased fluorescent intensities over a long period of time. The odorant sensor elements, based on Sf21 cell lines expressing insect odorant receptors, are sensitive to the level of several tens of parts per billion in solution. They can selectively distinguish between different types of odorants based on the odorant selectivity intrinsic to the expressed receptors and have response times of approximately 13 s. Specifically, using Sf21 cells and insect odorant receptors, the established cell lines

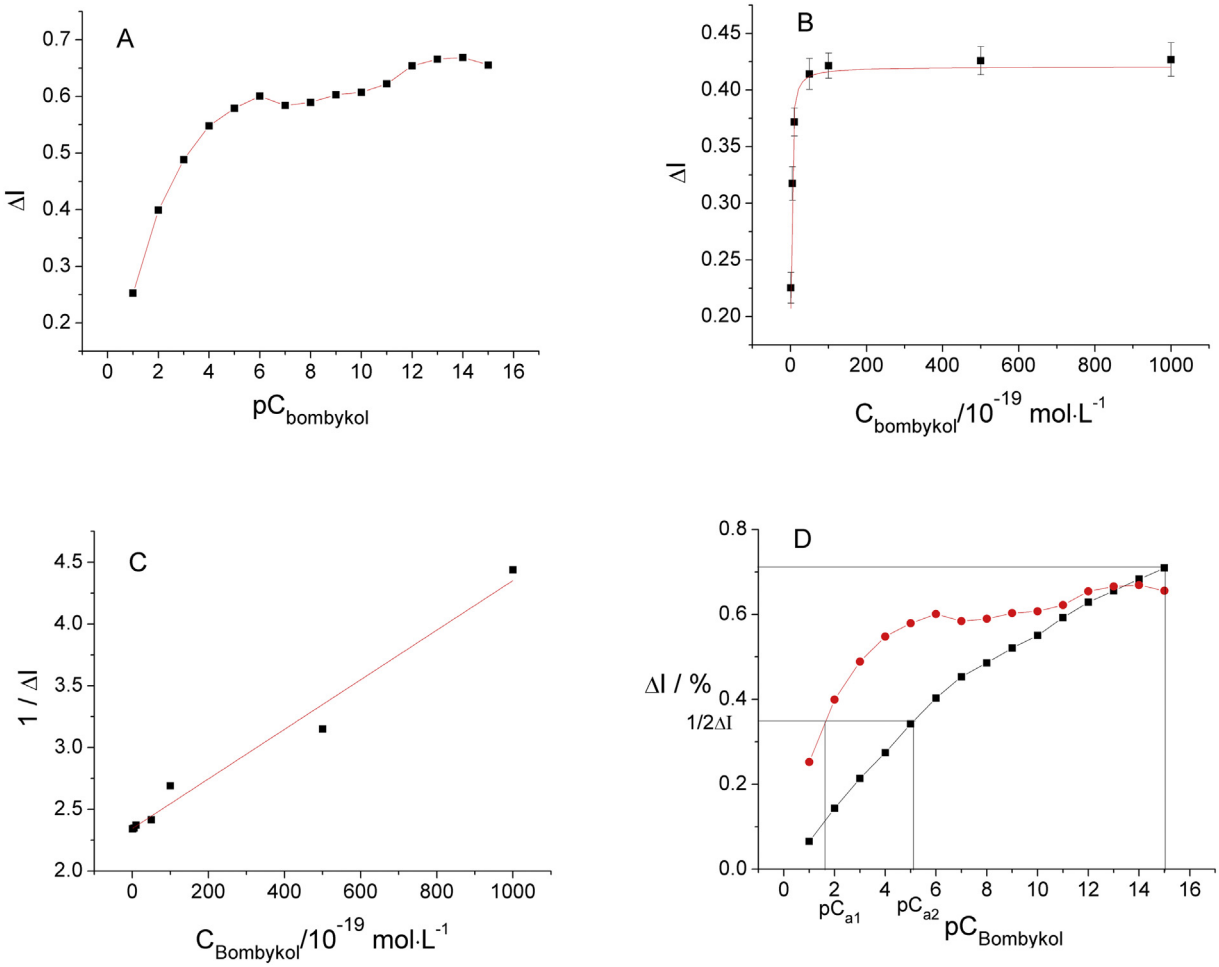

Fig. 5. (A) Current response values of bombykol in the detection range [10^{-19}–10^{-5} mol/L, $pC_{bombykol} = 20 + lg(C)$]. (B) The curve of interaction between bombykol (10^{-19}–10^{-16} mol/L) and receptor (the hyperbola fitting $R^2 = 0.9527$). (C) Plotting with double reciprocal: bombykol in the concentration range of 10^{-19}–10^{-16} mol/L; and (D) diagram of the signal amplification time calculation. The black line represents the bare electrode and the red line represents the prepared sensor.

stably expressing insect odorant receptors were found to detect odorants with consistent responsiveness for at least 2 months, thus exceeding the short lifespan normally associated with cell-based sensors. [31] Proteins from silkworm antenna were directly extracted in this study to act as the connecting molecule on the biosensor surface and initially applied for measuring bombykol response current and studying receptor–ligand interaction pattern. The biosensor displayed both hypersensitivity and hyperstability (long-term stability allowing for consistent detection of odorants, after culturing for days to months).

3.6. Biosensor signal magnification/stability/reproducibility and the service life of biosensors

The signal magnification was defined as follows: the ratio of receptor–ligand interaction/the same ligand–bare electrode interaction, upon 1/2 maximum response current to evaluate the performance of biosensor signal amplification system (Fig. 5D).

Signal magnification could be calculated using the following equation:

$$N = 10^{[pC_{a2} - pC_{a1}]} \quad (15)$$

The signal magnification of the proposed biosensor was about 10,000.

The BmOR1 biosensor was consecutively tested 12 times in the solution of 10^{-15} mol/L bombykol for every 15 min of incubation. The relative standard deviation (RSD) for the change rate of response currents was 4.3%, implying the proper stability of this biosensor.

This receptor biosensor was preserved at 4 °C in PBS and tested every 3 days at the same concentration of bombykol solution (10^{-15} mol/L). Biosensor response currents were basically stable for the first 21 days, whereas they were 82.3% of the initial current on the 24th day and only 42.8% on the 30th day, indicating that the electrochemical receptor biosensor could be preserved for at least 24 days. When five BmOR1 biosensors from different batches were tested at the same bombykol concentration (10^{-15} mol/L), the RSD of response currents was 5.14%, indicating proper reproducibility of this receptor biosensor. This was the first time BmOR1 was immobilized on a sensor surface to enable the ultrasensitive detection of bombykol. No data on bombykol electrochemical receptor biosensor have been reported so far. The detection of bombykol is generally carried out using Gas Chromatography-Mass Spectrometer (GC–MS) and Liquid Chromatography-Mass Spectrometer (LC-MS). Compared with GC–MS and LC-MS, electrochemical sensors have fast response, high sensitivity, and low cost.

3.7. Reaction kinetics between the bombykol electrochemical olfactory receptor biosensor and the nontarget compound

The bombykol electrochemical olfactory receptor biosensor was used to determine the current response of four bombykol analogs (Z11–16:Ald; Z11–16:OH; 16:OH; and Z9–16:Ald) in the concentration

range of 10^{-18}–10^{-10} mol/L. The logarithmic value of the corresponding compound concentration was plotted on the abscissa, and the current change rate of the response current was plotted on the ordinate (Fig. 6). The results showed that the sensor had good specificity.

3.8. Analysis of real samples

A recovery experiment was used to evaluate the accuracy of the method. The bombykol concentrations in three rat serum samples were tested under the best condition, and the bombykol standard solution was added to the serum. Finally, the bombykol concentration was measured. The test was repeated five times, and the recovery rates were between 96.7% and 104.5% (Table 2). This suggested that the accuracy of the method was good, which could be used to detect bombykol in real samples.

Table 2
Results of the recovery test of bombykol in rat serum samples ($n = 5$).

Sample	Concentration of bombykol (fmol/L)	Added (fmol/L)	Found (fmol/L)	Recovery (%)
1	3.36	20	24.4	104.5
2	1.87	20	22.7	103.8
3	6.79	20	25.9	96.7

4. Conclusions

In the present study, the BmOR1 was used as the test element, and Chit with good biocompatibility was used to absorb/immobilize AuNPs. Nanogold with the excessive specific surface area and good electrical conductivity self-assembled with BmOR1, which subsequently immobilized electron mediators with good performance (thiol groups and HRP) of the nanogold signal amplification system. Thus, a bilayer nanogold-modulated electrochemical sensor was prepared. Next, the amperometric *I–T* curve was adopted to measure the response current on its interaction with bombykol, and the BmOR1–bombykol interaction pattern was uncovered by analyzing the current change rate, with detection sensitivity reaching 10^{-19} mol/L. Furthermore, BmOR1 signal amplification constant *Ka* (8.57×10^{-20} mol/L) was calculated by simulating the enzyme kinetic equation, with a signal magnification of about 10,000-fold. This method was independent of the tissue or cell system and enabled the simulation of intracellular signal transduction with a novel signal transduction system, showing good performances. After stable preservation for 20 days, the biosensor still maintained 82.3% of the initial current, thereby overcoming the problem of a typical short lifespan associated with cell-based biosensors, such as odorant sensors using *Xenopus* oocytes [30]. After immobilizing the BmOR1 to the biosensor, the subsequent simulation of intracellular receptor signal cascade by the electrochemical signal amplification system helped in directly measuring the BmOR1–bombykol ligand interaction and exploring the kinetics. This biosensor provided a novel platform for studying receptor–ligand interactions.

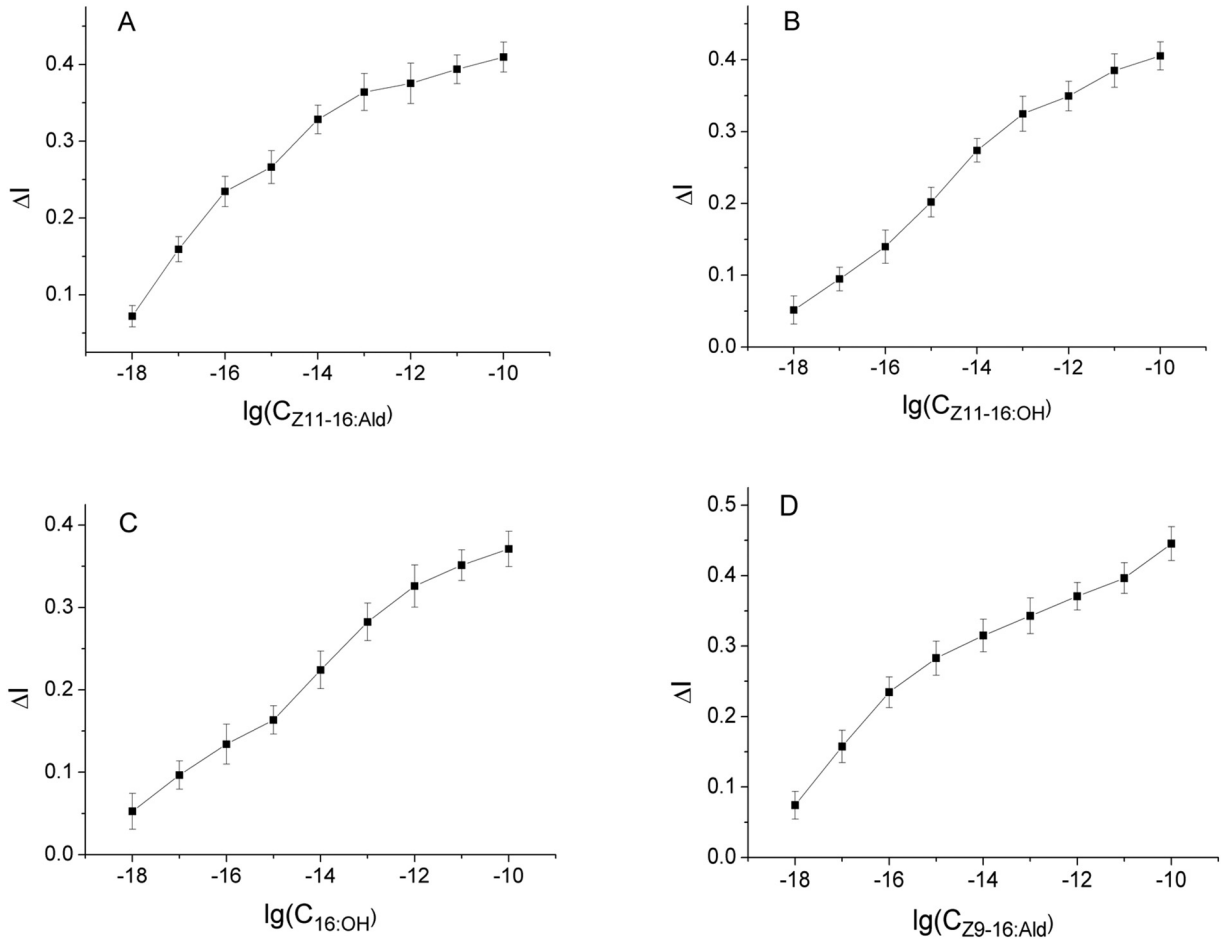

Fig. 6. Response currents Z11–16:Ald (A); Z11–16:OH (B); 16:OH (C); Z9–16:Ald (D); concentration range of 10^{-18}–10^{-10} mol/L in bombykol electrochemical olfactory receptor biosensor.

Acknowledgments

This study was financially supported by the National Science Foundation of China (Grant nos. 31671857 and 31371773).

Author contributions

Guangchang Pang conceived of and designed the experiments. Dingqiang Lu and Qiuda Xu performed the experiments and wrote the manuscript.

Conflicts of Interest

The authors declare no conflicts of interest.

References

[1] K. Yasumasa, M. Naoki, Y. Shigeki, N. Tadashi, Evaluation of Bombykol as the sex pheromone of *Bombyx mandarina* (Lepidoptera: Bombycidae), Jpn. J. Appl. Entomol. Zool. 19 (1984) 265–267, https://doi.org/10.1303/aez.19.265.
[2] Y. Gong, T.C. Pace, C. Castillo, C. Bohne, M.A. O'Neill, E. Plettner, Ligand-interaction kinetics of the pheromone- binding protein from the gypsy moth, l. dispar: insights into the mechanism of binding and release, Chem. Biol. 16 (2009) 162–172, https://doi.org/10.1016/j.chembiol.2009.01.005.
[3] A. Butenandt, R. Beckamnn, E. Hecker, Über den Sexuallockstoff des Seidenspinners.1. Der biologische Test und die Isolierung des reinen Sexuallockstoffes Bombykol, Hoppe Seyler's Z. Physiol. Chem. 324 (1961) 71–83, https://doi.org/10.1515/bchm2.1961.324.1.71.
[4] D. Wicher, R. Schafer, R. Bauernfeind, M.C. Stensmyr, R. Heller, S.H. Heinemann, B.S. Hansson, Drosophila odorant receptors are both ligand-gated and cyclic-nucleotide-activated cation channels, Nature 452 (2008) 1007–1011, https://doi.org/10.1038/nature06861.
[5] T.S. Ha, D.P. Smith, Insect odorant receptors: channeling scent, Cell 133 (2008) 761–763, https://doi.org/10.1016/j.cell.2008.05.007.
[6] A.J. Venkatakrishnan, X. Deupi, G. Lebon, C.G. Tate, G.F. Schertler, M.M. Babu, Molecular signatures of G-protein-coupled receptors, Nature 494 (2013) 185–194, https://doi.org/10.1038/nature11896.
[7] N.F. Brito, M.F. Moreira, A.C.A. Melo, A look inside odorant-binding proteins in insect chemoreception, J. Insect Physiol. 95 (2016) 51–65, https://doi.org/10.1016/j.jinsphys.2016.09.008.
[8] Q. Liu, W. Liu, B. Zeng, G. Wang, D. Hao, Y. Huang, Deletion of the Bombyx mori odorant receptor co-receptor (BmOrco) impairs olfactory sensitivity in silkworms, Insect. Biochem. Mol. 86 (2017) 58–67, https://doi.org/10.1016/j.ibmb.2017.05.007.
[9] S. Ihara, K. Yoshikawa, K. Touhara, Neuroscience forefront review: chemosensory signals and their receptors in the olfactory neural system, Neuroscience 254 (2013) 45–60, https://doi.org/10.1016/j.neuroscience.2013.08.063.
[10] R. Fredriksson, M.C. Lagerström, L.G. Lundin, H.B. Schiöth, The G-protein-coupled receptors in the human genome form five main families phylogenetic analysis, paralogon groups, and fingerprints, Mol. Pharmacol. 63 (2003) 1256–1272, https://doi.org/10.1124/mol.63.6.1256.
[11] S.A.M. Martins, J.R.C. Trabuco, G.A. Monteiro, V. Chu, J.P. Conde, D.M.F. Prazeres, Towards the miniaturization of GPCR-based live-cell screening assays, Trends Biotechnol. 30 (2012) 566–574, https://doi.org/10.1016/j.tibtech.2012.07.004.
[12] M.L. Yarmush, K.R. King, Living-cell microarrays, Annu.Rev. Biomed. Eng. 11 (2009) 235–257, https://doi.org/10.1146/annurev.bioeng.10.061807.160502.
[13] W.M. Hsien, S.B. Huang, G.B. Lee, Microfluidic cell culture systems for drug research, Lab Chip 10 (2010) 939–956, https://doi.org/10.1039/b921695b.
[14] T. Reisine, A. Gilchrist, R.M. Eglen, The use of immortalized cell lines in GPCR screening: the good, bad and ugly, Comb. Chem. High. Throughput Screen. 11 (2008) 560–565, https://doi.org/10.2174/138620708785204144.
[15] I. Navratilova, J. Besnard, A.L. Hopkins, Screening for GPCR ligands using surface Plasmon resonance, ACS Med. Chem. Lett. 2 (2011) 549–554, https://doi.org/10.1021/ml2000017.
[16] C.A. Shepherd, A.L. Hopkins, I. Navratilova, Fragment screening by SPR and advanced application to GPCRs, Prog. Biophys. Mol. Biol. 116 (2014) 113–123, https://doi.org/10.1016/j.pbiomolbio.2014.09.008.
[17] C.W. Scott, M.F. Peters, Label-free whole-cell assays: expanding the scope of GPCR screening, Drug Discov. Today 15 (2010) 704–716, https://doi.org/10.1016/j.drudis.2010.06.008.
[18] M. Saitakis, E. Gizeli, Acoustic sensors as a biophysical tool for probing cell attachment and cell/surface interactions, Cell. Mol. Life Sci. 69 (2012) 357–371, https://doi.org/10.1007/s00018-011-0854-8.
[19] P. Zijlstra, P.M.R. Paulo, M. Orrit, Optical detection of single non-absorbing molecules using the surface plasmon resonance of a gold nanorod, Nat. Nanotechnol. 7 (2012) 379–382, https://doi.org/10.1038/nnano.2012.51.
[20] L. Wei, L. Qiao, G. Pang, J. Xie, A kinetic study of bitter taste receptor sensing using immobilized porcine taste bud tissues, Biosens. Bioelectron. 92 (2017) 74–80, https://doi.org/10.1016/j.bios.2017.01.064.
[21] P. Rau, N. Rau, The sex attraction and rhythmic periodicity in giant saturniid moths, Trans. Acad. Sci. St. Louis 26 (1929) 83–221.
[23] L. Gerbino, J. Riva, M. Strumia, R.A. Iglesias, A.M. Baruzzi, Thionine immobilized in crosslinked chitosan films, Sensors Actuators B Chem. 131 (2008) 455–461, https://doi.org/10.1016/j.snb.2007.12.006.
[24] G. Frens, Controlled nucleation for the regulation of the particle size in monodisperse gold suspensions, Nat. Phys. Sci. 241 (1973) 20–22, https://doi.org/10.1038/physci241020a0.
[25] X. Kang, G. Pang, X. Liang, M. Wang, J. Liu, W. Zhu, Study on a hydrogen peroxide biosensor based on horseradish peroxidase/GNPs-thionine/chitosan, Electrochim. Acta 62 (2012) 327–334, https://doi.org/10.1016/j.electacta.2011.12.034.
[26] X. Kang, G. Pang, Q. Chen, X. Liang, Fabrication of Bacillus cereus electrochemical immunosensor based on double-layer gold nanoparticles and chitosan, Sensors Actuators B Chem. 177 (2013) 1010–1016, https://doi.org/10.1016/j.snb.2012.12.018.
[27] D. Lu, G. Pang, J. Xie, A new phosphothreonine lyase electrochemical immunosensor for detecting *Salmonella* based on horseradishperoxidase/GNPs-thionine/chitosan, Biomed. Microdevices 19 (2017) 1–10, https://doi.org/10.1007/s10544-017-0149-4.
[28] S. Kang, K.K. Shiu, Scanning tunneling microscopic and voltammetric studies of the surface structures of an electrochemically activated glassy carbon electrode, Anal. Chem. 74 (2002) 879–885, https://doi.org/10.1021/ac010734+.
[29] T. Nagaoka, T. Yoshino, Surface properties of electrochemically pretreated glassy carbon, Anal. Chem. 58 (1986) 1037–1042, https://doi.org/10.1021/ac00297a012.
[30] N. Misawa, H. Mitsuno, R. Kanzaki, S. Takeuchi, Highly sensitive and selective odorant sensor using living cells expressing insect olfactory receptors, Proc. Natl. Acad. Sci. U. S. A. 107 (2010) 15340–15344, https://doi.org/10.1073/pnas.1004334107.
[31] H. Mitsuno, T. Sakurai, S. Namiki, H. Mitsuhashi, R. Kanzaki, Novel cell-based odorant sensor elements based on insect odorant receptors, Biosens. Bioelectron. 65 (2015) 287–294, https://doi.org/10.1016/j.bios.2014.10.026.